RIS-Aided Secure Millimeter-Wave Communication Under RF-Chain Impairments

Mohammad Ragheb, Ali Kuhestani, *Member, IEEE*, Mohammad Kazemi, *Member, IEEE,* Hossein Ahmadi, *Student Member, IEEE,*, and Lajos Hanzo, *Life Fellow, IEEE*

Abstract—The effects of hardware impairments (HWIs) on the secrecy performance of a reconfigurable intelligent surface (RIS)-assisted millimeter wave system are investigated, where a multi-antenna base station (BS) transmits confidential messages to a single-antenna mobile user (MU) in the presence of a single-antenna passive eavesdropper (Eve). Artificial noise (AN)-aided transmission by the BS is proposed for improving the achievable secrecy rate. As the first step, we construct a system model in the absence of HWIs. For this case, we present optimal solutions for the signal and AN powers, the beamforming design at the BS, and the phase shifts of the RIS elements. Then closed-form expressions are derived for the cumulative distribution functions of the signal-to-noise-ratios experienced at the legitimate and eavesdropping nodes. Finally, a compact solution is presented for the ergodic secrecy rate (ESR) performance. At the next step, we extend our designs and analysis by considering the HWIs of the radio-frequency (RF) modules of the BS, MU and Eve. Our results highlight the detrimental impact of HWIs on the achievable ESR. Finally, we find that the ESR can be further increased by beneficially distributing the tolerable HWIs between the transmission and reception RF chains.

Index Terms—Physical layer security, intelligent reflecting surface, hardware impairments.

I. INTRODUCTION

With the advent of millimeter-wave (mmWave) communications, as a key enabling technology for next-generation wireless communications, Gigabytes per second data rates may become available. Since mmWave systems suffer from severe path losses compared to sub-6 GHz systems, large scale antenna arrays (LSAA) are commonly used for attaining considerable beamforming gains. Due to the inherent directivity in mmWave systems, their propagation is prone to blockage. Nevertheless, the statistical models of mmWave channels indicate the presence of Line-of-sight (LoS) and Non-Line-of-sight (NLoS) links [1]. In this environment, relaying plays a key role in the design of mmWave cellular networks,

M. Ragheb and H. Ahmadi are with the Electrical Engineering Department, Amirkabir University of Technology, Tehran, Iran (emails: mohammad_ragheb@aut.ac.ir; Hossein.Ahmadi@ieee.org)

A. Kuhestani is with the Communications and Electronics Department, Faculty of Electrical and Computer Engineering, Qom University of Technology, Qom 3716146611, Iran (e-mail: kuhestani@qut.ac.ir).

M. Kazemi is with the department of Electrical and Electronics Engineering, Bilkent University, Ankara, Turkey, (e-mail: kazemi@ee.bilkent.edu.tr)

L. Hanzo is with the University of Southampton, Southampton SO17 1BJ, U.K, (e-mail: hanzo@soton.ac.uk).

Corresponding author: Ali Kuhestani

and leads to improve of network coverage. However, is the extra power consumption of relay nodes justifyable in terms performance gains, when aiming for meeting the requirements of high data rates and massive wireless connectivity? Clearly, energy efficiency is a critical yet challenging issue in practical systems, and its improvement typically increases the hardware costs. Specifically, high-performance communication in the mmWave frequency bands relying on multiple input-multiple output (MIMO) schemes requires expensive radio-frequency (RF) arrays and complex signal processing. Additionally, adding further active components to a wireless network would increase the interference load. Therefore, recently much attention has been devoted to improving both bandwidth and energy efficiencies at a low hardware cost [2].

In a reflecting intelligent surface (RIS), a low cost passive structure is employed as an alternative to conventional relays, which digitally adjusts the received signal phase and sends it to the destination at a low power consumption [3]. To achieve a high beamforming gain at a low hardware/energy consumption, RIS has the benefit of improved spectrum utilization, coverage expansion, interference mitigation, and increased energy efficiency [4], [5]. Using a large intelligent surface, Han *et al.* [3], designed the optimal phase shifts based on the upper bound of the ergodic spectral efficiency by employing supplementary links between the source and the user, while assuming that there is no direct path between them. Wang *et al.* [6] used a rank-one geometric model for jointly optimizing the base station's (BS) transmit precoding (TPC) vector and phase shift parameters used by RISs for maximizing the received signal power at the user, and highlighted that the received signal power increases dramatically with the number of reflective elements. They have also shown that the RISs significantly mitigate the effects of blockage.

Since the signal broadcast in wireless communications is prone to interception, the security of information requires special measures. To address this critical issue, physical layer security (PLS) techniques have emerged as efficient and practical solutions in diverse communication scenarios [7]–[13]. In recent years, RIS-assisted secure transmissions [14]–[20] have also gained more attention as a benefit of the increased degree of freedom attained by RIS-assisted passive beamforming. To be specific, Cui *et al.* [15] have shown that the average secrecy rate increases significantly by increasing the transmit power, while the amount of information leaked to the eavesdropper (Eve) is reduced even when the eavesdropping channel is stronger than the legitimate channel. In fact by considering a challenging setup where the eavesdropping

channel is stronger than the legitimate communication channel, the method proposed in [15] is capable of significantly improving the performance, by exploiting the RIS-aided power enhancement at the legitimate receiver. Artificial noise (AN) can be employed to enhance the secrecy rate of the RIS-assisted wireless communication [16]. The results in [16] show that as the number of reflecting elements increases, the performance gain remains constant when the Eves are faraway from the IRS and it decreases when the Eves are close to the RIS. Additionally, the results in [17] proceed to maximize the secrecy rate of an RIS-aided transmission by proposing an efficient iterative algorithm for optimizing the covariance matrix of the signal transmitted by the source node, and the phase shift matrix of the RIS. In [20], a double-RIS assisted design for improving the secrecy performance of wireless transmission has been exploited. The authors in [20] proposed a numerical algorithm by considering the inter-surface signal reflection to maximize the secrecy rate. Due to the estimation mismatch and the passivity of Eves, perfect channel state information (CSI) of wiretap links is challenging to obtain. In mmWave cognitive radio networks (CRNs), Wu *et al.* [21] introduced an RIS into mmWave CRNs and designed a robust secure beamforming (BF) scheme. Egashira *et al.* [22] investigated the application of the hybrid relay-reflecting intelligent surface (HR-RIS) in improving the secrecy capacity of mmWave MIMO systems with the presence of multi-antenna Eve. For that purpose, the joint optimization of the transmit beamformer and the relay-reflecting coefficients at RIS tackled via alternating optimization.

One of the essential considerations in the design of wireless systems is the effect of hardware impairments (HWIs) such as I/Q imbalance, oscillator phase noise, high power amplifier nonlinearities, and quantization errors [11], [23], [24]. The severity of the impairments also depends on the quality of the hardware used in the RF transceivers. Recently, some authors have proposed PLS both for sub-6 GHz communications [11], [13], and for the mmWave bands [12]. Recently, Explicitly, Boulogeorgos *et al.* [13] investigated the detrimental impact of transceiver HWIs on the outage and ergodic capacity performance of RIS-assisted wireless systems without considering any security issues in the sub-6GHz bands.

Some authors as [25]–[27] have only considered the effect of transceiver HWIs or the HWIs of the RIS, while some other papers [28]–[34] have considered the effect of both imperfections on the performance of the systems. Li *et al.* [25] considered RIS-assisted wireless power transfer (WPT) for both perfect and imperfect phase adjustments in Rayleigh fading channels. For imperfect phase adjustments, they explained the effect of phase errors in the context of discrete phase shift quantization and derived the outage probability and symbol error rate (SER) equations. Trigui *et al.* [26] investigated a secure RIS-assisted communications in the presence of discrete phase shifts in the presence of colluding eavesdropping. The author of [27] investigated the impact of transceiver HWIs on the performance of RIS-assisted wireless systems. Specifically, they have analyzed the spectral efficiency (SE), the energy efficiency (EE), and the outage probability of RIS-assisted wireless systems by finding their closed-form expressions.

The simulation results revealed the importance of modeling and compensating the HWIs, as they considerably limit the performance of such systems. Papazafeiropoulos *et al.* [28] turned their attention to the design/study of a general RIS-assisted multi-user-multiple input-single output system having imperfect CSI and HWIs at both the RIS and the transceiver, while performing robust optimization. Dai *et al.* [29] consider a RIS-aided massive multi-user MIMO communication system in the face of transceiver HWIs and RIS phase noise. Nguyen *et al.* [30] considered the performance degradation of practical RIS-aided systems by quantifying the detrimental impact of in-phase and quadrature-phase imbalance (IQI). They demonstrated that the RIS with IQI and HWI achieves significant outage probability improvement at high SNRs, provided that the number of reflecting coefficients is sufficiently high. The authors of [31] focused their attention on the EE analysis of RIS-aided wireless systems, when the aggregate HWIs of the transceiver are modeled as independent additive noise and the HWIs of RIS are modeled by phase impairments. The authors of [32] present a unifying framework for future RIS-assisted space shift keying systems. The performance of the proposed scheme is expressed in terms of the theoretical average bit error rate, under the impact of non-ideal transceivers. Notably, the introduction of HWIs increases the complexity of the mathematical analysis of RIS-assisted systems [28]. Chen *et al.* [33] studied the robust transmission design for an RIS-aided covert communication system in the presence of transceiver and RIS HWIs. All the above works have investigated the performance of RIS-assisted systems in the face of HWIs in sub-6 GHz networks, by contrast, we analyze mmWave networks, which is more challenging. It is worth noting that considering the HWIs regarding RIS in such a way that the RIS with discrete phase shifters cannot achieve optimal phase shifts, and thus the legitimate user (Bob) suffers from phase shift quantization errors. By taking into account the availability of the statistical CSI of Eves, pointing errors caused by highly-directional THz antennas, and the phase shift quantization errors, Tota Khel *et al.* [34] derived new expressions for the secrecy capacity in both cases of colluding/non-colluding Eves. While the authors of [34] considered a single antenna, we used an LSSA system with optimal power allocation to improve the secrecy rate. Furthermore, Trigui *et al.* [26] have examined the secrecy performance of RIS-aided sub-6 GHz communications in the presence of colluding Eves, while we have conceived an AN transmission strategy for improving the secrecy performance of RIS-based mmWave networks under HWIs in the transceivers.

However, there is a paucity of literature on the PLS of RIS-aided mmWave communications with special emphasis on the associated HWIs. To fill this knowledge-gap, we design a secure transmission scheme for an RIS-aided mmWave communication in the presence of HWIs. In our system model, an LSAA-aided BS communicates with a single-antenna mobile user (MU) using an RIS having a large number of elements, where the direct paths between them are blocked and a passive Eve overhears the communications. By considering her around the MU. Accordingly, it is desirable to transmit both the data and AN towards the MU and Eve, respectively,

through the RIS. It is worth noting that Eve may indeed be a legitimate user belonging to the network, whose channel and distribution are known. This belongs to the class of active Eves, but even passive Eves' channels might be detectable, for example, by detecting their oscillator leakage by a sensitive state–of–the–art receiver. For instance, we can refer to [18], where Eve's channel and its distribution are known. Furthermore, it is reasonable to assume that the channel between BS and Eve, and the channel between the RIS and Eve, are known in the scenario when Eve is an active user in the system, but untrusted by the legitimate receiver [15]. Furthermore, Yu *et al.* in [35], assumed that Eve is between the transmitter and the legitimate receiver, and they stated that while the CSI of Eve is generally hard to acquire, the results in [35] serve as theoretical performance upper bounds for the system under study. These bounds and the insights gained from them can be used to guide the system design for the scenario when the CSI of Eve is not perfectly known. In this paper, we aim for maximizing the achievable secrecy rate by judiciously designing both the signal and AN powers, while optimizing both the TPC design at the BS and the phase shifts of the RIS elements. To improve the paper's readability, we have included a table for acronyms and abbreviations in Table I. The main contributions of this paper are boldly and explicitly contrasted to the literature in Table II at a glance. Our contributions are further detailed as follows:

- We commence by studying the system model in the absence of HWIs. For this case, we derive optimal solutions for the above mentioned parameters. Then closed-form expressions are derived for the cumulative distribution functions (CDFs) of the SNRs of both the legitimate and eavesdropping nodes. Finally, a compact solution is presented for the ergodic secrecy rate (ESR).
- At the next step, we consider having realistic HWIs at the BS, MU and Eve in their RF chains. Additionally, we find optimal solutions for the parameters of the system model. New closed-form expressions are derived for the CDFs of the SNRs of both the legitimate and eavesdropping nodes, which are necessary for arriving at a compact expression of the overall performance. Our simulation results show that the HWIs only have a modest effect on the ESR at low SNRs, while at high SNRs, their impact is more harmful.
- We also provide new insights for hardware design with the goal of maximizing the ESR. From an engineering perspective, the results reveal that the ESR can be improved by optimally distributing the level of HWIs between the BS transmitter and the MU receiver.

The rest of the paper is organized as follows. Section II presents our system model, signal model, the RIS-assisted system model that takes into account the effect of transceiver hardware imperfections and some of our assumptions. The problem formulation and the channel model is introduced and the related OPA is evaluated. In Section III we proceed to find the optimal solution. For this purpose we design and analysis the ESR of RIS-assisted mmWave systems in the context of perfect hardware and then the impact of HWIs imposed on

RIS-assisted mmWave systems is investigated. In section IV, we turn our attention to the RF imperfections of an RIS-assisted network for maximizing the ESR. Section V discusses our simulation results. Finally, we conclude in Section VI. The notations are summarized in Table III.

II. SYSTEM AND SIGNAL MODEL

As illustrated in Fig. 1, the system model under investigation is the RIS-assisted large-scale antenna aided mmWave downlink, consisting of a multiple-antenna transmitter Alice (A) having an N elements in a large uniform linear array (ULA), a single-antenna receiver Bob (B) and a single-antenna Eavesdropper (Eve or E). The RIS is positioned between A as well as B and contains M reflecting elements arranged in a ULA. We assume that there is no direct link between A and B due to the blockage, hence only the RIS can establish their communication. [1] Eve is assumed to be in the communication range of both A and B for gleaning confidential information from the reflected channels. In our model, Alice transmits AN through the null-space of the Alice-to-RIS-to-Bob channel for confusing Eve. Hence, in this case, Eve can be passive. Furthermore, the power allocation factor between the signal message and AN is optimized. The RIS has up to M low-cost configurable reflective elements and each element independently reflects the phase shifted version of the input signal, thus increasing the quality of the signal received by the B while reducing data leakage to Eve. An intelligent controller beneficially adjusts the phase shifts of the passive RIS elements. To elaborate a little further, the controller coordinates and manages both A and the RIS for channel learning and data transmission via fiber links [3], [40]. We note that although RIS-aided communications introduce some delay, it may be deemed negligible compared to the duration of the actual data transmission [18], [38]. Considering this assumption, as shown in Fig. 1, Alice transmits her own data to the RIS, which reflects received signals at a negligible delay. The channel vectors between A and the RIS, and the RIS as well as B are denoted by $\mathbf{H}_{\mathrm{AI}} \in C^{M \times N}$ and $\mathbf{h}_{\mathrm{IB}} \in C^{M \times 1}$, respectively. The channel vectors between A and E, as well as the RIS and E are denoted by $\mathbf{h}_{\mathrm{AE}} \in C^{N \times 1}$ and $\mathbf{h}_{\mathrm{IE}} \in C^{M \times 1}$, respectively. Let $\theta_{\mathrm{l,m}} \in [0, 2\pi]$ denote the phase shift of the reflecting coefficient of the m-th element, which is defined as

$$\boldsymbol{\theta} = \mathrm{diag}(e^{\mathrm{j}\theta_1}, e^{\mathrm{j}\theta_2}, ..., e^{\mathrm{j}\theta_{\mathrm{M}}}). \tag{1}$$

Let $\boldsymbol{W} \in C^{N \times 1}$ denote the TPC vector used by A. The information signal is sent by A at the power of λP to the RIS, and concurrently A radiates AN at the power of $(1-\lambda)P$

---

[1]We note that the model proposed in [28] assumes the presence of a direct link between the BS and the MUs, but highlights that these may be neglected in certain scenarios. For example, in mmWave transmission, the associated high penetration losses and resultant signal blockages tend to attenuate the LoS component [37]. Hence, inspired by the authoritative literature including [13], [18], [19], [38], and [39], we assumed that the direct link between the transmitter and receiver is sufficiently weak to be ignored due to obstacles and/or deep fading. For further description, Cao *et al.* [39] assumed that a BS is a dedicated access point (AP) that only communicates with the RIS, since the mmWave links between the BS and MUs are highly susceptible to environmental blockages.

TABLE I: List of acronyms and abbreviations.

Variable	Description	Variable	Description
A	Alice	HWIs	Hardware impairments
AN	Artificial noise	IQI	In-phase and quadrature-phase imbalance
AoA	Azimuth angle of arrival	LoS	Line-of-sight
AoD	Azimuth angle of departure	LSAA	Large scale antenna arrays
AP	Access point	MIMO	Multiple input-multiple output
AWGN	Additive white Gaussian noise	mmWave	millimeter-wave
B	Bob	MRT	Maximum ratio transmission
BS	Base station	MU	Mobile user
CDF	Cumulative distribution function	NLoS	non-line-of-sight
CSI	Chnnel state information	OF	Objective function
EE	Energy efficiency	OPA	Optimal power allocation
EPA	Equal power allocation	PLS	Physical layer security
ESR	Ergodic secrecy rate	RF	Radio-frequency
Eve or E	Eavesdropper	RIS	Reconfigurable intelligent surface
EVM	Error vector magnitude	SE	Spectral efficiency
FPA	Full power allocation	TPC	Transmit precoding vector

TABLE II: Comparison between our contributions and the RIS-based mmWave communication.

Contributions	This work	[19]	[36]	[21]	[33]	[34]	[22]
Secrecy requirement	✓	✓	✓	✓		✓	✓
LSAA at BS (Alice)	✓						
AN injection	✓						
Network optimization with closed-form solutions	✓						
CDF evaluation of links	✓					✓	
Presence of HWIs	✓				✓		

TABLE III: NOTATIONS

Notation	Description
$\boldsymbol{H}_{\mathrm{AI}}$	The channel between the transmitter and the RIS
$\boldsymbol{h}_{\mathrm{IB}}$	The channel vector between the RIS and the receiver
$\boldsymbol{h}_{\mathrm{AE}}$	The channel vector between the transmitter and the IRS
$\boldsymbol{h}_{\mathrm{IE}}$	The channel between the IRS and the Eve
x_{s}	The unit power information signal (the desired signal power with unit power)
x_{z}	The unit power jamming signal (the jamming signal power with unit power)
$\theta_{\mathrm{l,m}}$	The phase shift of the reflecting coefficient of the m-th element from l-th path
$\boldsymbol{W}$	TCP vector used by the transmitter
$\boldsymbol{W}_2$	The TCP vector designed for the AN
λ	The power sharing factor
$\boldsymbol{\eta}_{\mathrm{A}}$	The distortion caused by HWIs in the transmitter
$\eta_{\mathrm{j}}, j \in \{B, E\}$	The distortion noise in the receiver with zero mean and the variance of σ_{j}^2
$\kappa_{\mathrm{j}}, j \in \{A, B, E\}$	The level of impairment in the j-th channel. The parameter can be interpreted as the total EVM
y_{B}	The received signal at the receiver
y_{E}	The received signal at the Eve
$n_{\mathrm{j}}, j \in \{B, E\}$	The additive white Gaussian noise (AWGN) at the receiver or Eve
N	Number of antennas at the transmitter. (The transmitter having an N elements in a large uniform linear array)
M	Number of reflecting elements arranged in a ULA. (The RIS contains an M elements in a large uniform linear array)
R_{s}	The instantaneous secrecy rate
$\bar{R}_{\mathrm{s}}^{\mathrm{P}}$	The ESR of the perfect hardware
$\bar{R}_{\mathrm{s}}^{\mathrm{IP}}$	The ESR of the imperfect hardware

toward the Eve for contaminating the intercepted signal, where $\lambda \in [0, 1]$ is the power sharing factor.

The HWIs at A cause a mismatch between the intended transmitted signal, and what is actually generated. Upon denoting the distortion caused by HWIs in A by $\boldsymbol{\eta}_{\mathrm{A}}$, we model it by a complex Gaussian process having zero-mean as [11]

$$\boldsymbol{\eta}_{\mathrm{A}} \sim \mathcal{CN}\left(\boldsymbol{0}, \frac{\lambda P \kappa_{\mathrm{A}}^2}{\|\boldsymbol{h}_{\mathrm{AIB}}\|^2}\mathrm{diag}(|h_{\mathrm{AIB}_1}|^2...|h_{\mathrm{AIB_N}}|^2)\right). \quad (2)$$

In (2), $\boldsymbol{h}_{\mathrm{AIB}}$ denotes the channel between A and B via the RIS, which is defined later, and k_{A} represents A's error vector magnitude (EVM)—a common measure for quantifying the quality of RF transceivers, which is a non-negative design parameter [13].

At B and Eve, similar to [11, eq. (2) and eq. (3)], the received signals can be written respectively as follows

$$y_{\mathrm{B}} = \sqrt{\lambda P}\boldsymbol{h}_{\mathrm{IB}}^{\mathrm{H}}\boldsymbol{\theta}\boldsymbol{H}_{\mathrm{AI}}\boldsymbol{W}x_{\mathrm{s}} + \boldsymbol{h}_{\mathrm{IB}}^{\mathrm{H}}\boldsymbol{\theta}\boldsymbol{H}_{\mathrm{AI}}\boldsymbol{\eta}_{\mathrm{A}} + \eta_{\mathrm{B}} + n_{\mathrm{B}}, \quad (3)$$

$$y_{\mathrm{E}} = \sqrt{\lambda P}\boldsymbol{h}_{\mathrm{IE}}^{\mathrm{H}}\boldsymbol{\theta}\boldsymbol{H}_{\mathrm{AI}}\boldsymbol{W}x_{\mathrm{s}} + \sqrt{(1-\lambda)P}\boldsymbol{h}_{\mathrm{IE}}^{\mathrm{H}}\boldsymbol{\theta}\boldsymbol{H}_{\mathrm{AI}}\boldsymbol{W}_2 x_{\mathrm{z}}$$
$$+ \boldsymbol{h}_{\mathrm{IE}}^{\mathrm{H}}\boldsymbol{\theta}\boldsymbol{H}_{\mathrm{AI}}\boldsymbol{\eta}_{\mathrm{A}} + \eta_{\mathrm{E}} + n_{\mathrm{E}}. \quad (4)$$
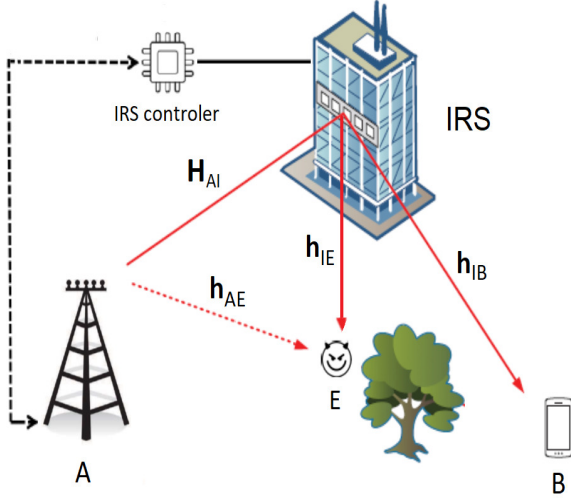
Fig. 1: Secure communication in a cooperative mmWave system model in the presence of RIS and a passive Eve.

In, (3) and (4), x_s is the desired signal with unit power, W and W_2 are the TPC vectors designed for the desired signal and for the AN, respectively. The AN bearing signal x_z is considered have $\sigma_z^2 = 1$. Furthermore, $n_j \sim (0, \sigma_0^2)$, $j \in \{B, E\}$ are the additive white Gaussian noise (AWGN) at B or E. Note that η_j, $j \in \{B, E\}$, is the distortion noise in the receiver and is modeled as $\eta_j \sim \mathcal{CN}\left(0, \lambda P \kappa_j^2 \|\boldsymbol{h}_{AIj}\|^2\right)$ [11] where the Gaussianity is due to the aggregate effect of many impairments. The parameter $\kappa_j > 0$, $j \in \{A, B, E\}$, describes the level of impairments on the j-th channel. Note that κ_j can be interpreted as the total EVM. This parameter is essentially constant while operating in the dynamic range of the power amplifier. [2] Furthermore, η_j $j \in \{B, E\}$ represents the distortions resulting from HWIs of node j and are modeled as complex Gaussian processes with zero-mean and the variance of

$$\sigma_{\eta_j}^2 = \lambda P k_j^2 \|\boldsymbol{h}_{Ij}^H \boldsymbol{\theta} \boldsymbol{H}_{AI}\|^2, j \in \{B, E\}, \quad (5)$$

where k_B and k_E represent the B's and E's EVM, respectively.

Remark 1: Again, some papers such as [13], [27] and [41], have only considered the effect of transceiver HWIs. The above papers also assumed that the RIS is completely aware of the phase of the BS $\rightarrow$ RIS channel and the phase of the RIS $\rightarrow D_k$ (legitimate receiver k)/Eve channel, and hence chooses the best phase shift. Hence in like with these, only considered the effect of transceiver HWIs in our paper. As such some other papers, including [42] considered the effect of both imperfections on the performance of the systems.

By considering (3), the received signal-to-interference-plus-noise ratio (SINR) at B is

$$\gamma_B = \frac{\lambda P |\boldsymbol{h}_{IB}^H \boldsymbol{\theta} \boldsymbol{H}_{AI} \boldsymbol{W}|^2}{|\boldsymbol{h}_{IB}^H \boldsymbol{\theta} \boldsymbol{H}_{AI} \boldsymbol{\eta}_A|^2 + \sigma_{\eta_B}^2 + \sigma_0^2}. \quad (6)$$

By substituting (2), and (5) into (6) and considering [12, Sec. (3)], (6) is written as

$$\gamma_B = \frac{\lambda \rho U_B}{\lambda \rho (k_A^2 + k_B^2) U_B + 1}, \quad (7)$$

where

$$U_B = \|\boldsymbol{h}_{IB}^H \boldsymbol{\theta} \boldsymbol{H}_{AI}\|^2, \quad (8)$$

and $\rho = \frac{P}{\sigma_0^2}$.

Using (4), the signal received at E becomes

$$\gamma_E = \frac{\lambda \rho U_E}{(1-\lambda)\rho U_{AE} + \lambda \rho (k_A^2 + k_E^2) U_E + 1}, \quad (9)$$

where

$$U_{AE} = |\boldsymbol{h}_{AE}^H \boldsymbol{W}_2|^2, \quad (10)$$

and

$$U_E = |\boldsymbol{h}_{IE}^H \boldsymbol{\theta} \boldsymbol{H}_{AI} \boldsymbol{W}|^2, \quad (11)$$

which is obtained assuming that E is located near B which is the worst case in terms of secrecy and using the approximation $|\boldsymbol{h}_{IE}^H \boldsymbol{\theta} \boldsymbol{H}_{AI} \boldsymbol{W}|^2 \approx |\boldsymbol{h}_{IE}^H \boldsymbol{\theta} \boldsymbol{H}_{AI}|$.

III. SECRECY EVALUATION AND PROBLEM FORMULATION

Before proceeding this section we have provided a diagram, depicted in Fig. 2, to show the flow of the analysis described in the sequel. This diagram facilitates the legibility of this paper for the readers to know, what comes next in this paper. In this section, we evaluate the ESR of RIS-assisted mmWave networks. The level of PLS is generally characterized in terms of its secrecy rate, R_s, as

$$R_s = [\log_2(\frac{1+\gamma_B}{1+\gamma_E})]^+, \quad (12)$$

where $[x]^+ = \max\{x, 0\}$. Furthermore, the ESR is calculated as $\bar{R}_s = \mathbb{E}\{R_s\}$, where $\mathbb{E}[.]$ denotes the expectation. We present both an alternating power optimization technique and active as well as passive beamforming design. We first start with our OPA strategy. By defining $\varphi(\lambda) = \frac{1+\gamma_B(\lambda)}{1+\gamma_E(\lambda)}$, we have the following key proposition.

Proposition 1: For a large-antenna A and an RIS having numerous elements, the function $\varphi(\lambda)$ is a quasi-concave function of λ in the feasible set, and the solution, which is denoted as the OPA, is given by

$$\lambda^* = \frac{1}{1+\sqrt{\frac{U_E}{U_{AE}}(1+\rho U_B(k_A^2 + k_B^2))}}. \quad (13)$$

$$\varphi(\lambda^*) = \frac{1 + \rho U_B + \sqrt{\frac{U_E}{U_{AE}}\left(1 + \rho U_B(k_A^2 + k_B^2)\right)}}{\left(1 + \sqrt{\frac{U_E}{U_{AE}}\left(1 + \rho U_B(k_A^2 + k_B^2)\right)}\right)^2} \quad (14)$$

Step 0.   **Main objective:**

Maximizing the instantaneous secrecy rate (R_s) shown in (12)

Step 1.   **OPA factor design:**

Calculating the OPA parameter (λ^*) in the function of $\varphi(\lambda)$. By substituting λ^* into $\varphi(\lambda)$ and after some further mathematical operations, we arrive at a streamlined equation for $\varphi(\lambda)$ like (18) for perfect hardware and like (33) for imperfect hardware.

Step 2.   **Optimal Solution and Performance Analysis for Optimizing W:**

We solve the Problem (19) for perfect hardware analysis by optimizing W and θ alternatively and a similar problem is designed for imperfect hardware analysis.

For a fixed θ, the maximized ESR, is given by W^* in Eq. (23).

Step 3.   **Optimal Solution and Performance Analysis for Optimizing θ:**

We solve the respective Problems in step 2 for optimizing θ. Then the optimal θ^* is formulated in Eq. (24) that maximizes R_s.

Step 4.   **CDFs calculation:**

The CDF of the random variables U_B (Eq. (25)), U_E (Eq. (27)) and U_{AE} (Eq. (29)) are calculated. As such, this leads to extracting the CDFs of some variables like $\sqrt{\frac{U_E}{U_{AE}}}$ and $\sqrt{\frac{U_E}{U_{AE}}}U_E$.

Step 5.   **Calculating the ESR:**

The ESR of the perfect and imperfect hardware associated with AN-aided transmission via the RIS can be calculated as seen in (32) and (35).

Fig. 2: Flow of mathematical analysis.

Proof: By substituting (7), and (9) into $\varphi(\lambda)$ and taking its derivative with respect to λ, we obtain

$$\varphi'(\lambda) = \frac{\lambda^2[U_{AE} - U_E - \rho U_B U_E(k_A^2 + k_B^2)] - 2\lambda U_{AE} + U_{AE}}{[\lambda\rho(k_A^2 + k_B^2)U_B + 1]^2[(1 - \lambda)\rho U_{AE} + \lambda\rho U_{AE}]^2}. \tag{15}$$

Proof. Since $\varphi'(0) > 0$, $\varphi'(\lambda^*) = 0$, and $\varphi'(1) < 0$, we conclude that $\varphi(\lambda)$ is a quasi-concave function in the feasible set. By setting $\varphi'(\lambda)$ to zero, the single feasible solution is obtained as (13). ∎

As it can be deduced from (13), for a system having HWIs compared to its counterpart with no HWI, the value of λ^* is lower and it is inversely related to ρ.

Remark 2: Upon substituting (7) and (9) into the function $\varphi(\lambda)$, we can observe that in the numerator of $\varphi(\lambda)$, the term

$U_{AE} - U_E(k_A^2 + k_E^2)$ appears. Since AN is transmitted towards E, the RIS output is a signal focusing on the legal receiver, and $(k_A^2 + k_E^2)$ is a small factor, we conclude that $U_{AE} \gg U_E(k_A^2 + k_E^2)$. Then, for simplicity, the term $U_E(k_A^2 + k_E^2)$ is ignorable compared to U_{AE}. It is worth noting that in our scheme $\varphi(\lambda)$ does not depend on the HWIs at E, i.e., k_E.

In the following, we first design and analysis the ESR of RIS-assisted mmWave systems in the context of perfect hardware. Then the impact of HWIs imposed on RIS-assisted mmWave systems is investigated.

A. Perfect Hardware Analysis

For the analysis of perfect hardware in (13), we set $k_A = k_B = 0$, so the OPA factor becomes

$$\lambda^* = \frac{1}{1 + \sqrt{\frac{U_E}{U_{AE}}}}. \tag{16}$$

Upon substituting (16) into the function $\varphi(\lambda)$, we obtain

$$\varphi(\lambda^*) = \frac{1 + \rho U_B + \sqrt{\frac{U_E}{U_{AE}}}}{(1 + \sqrt{\frac{U_E}{U_{AE}}})^2}. \tag{17}$$

By injecting the AN, the value of U_{AE} becomes more significant than U_E, so we can neglect $\sqrt{\frac{U_E}{U_{AE}}}$ with respect to ρU_B in the numerator of (17). In other words, since $\rho U_B \gg \sqrt{\frac{U_E}{U_{AE}}}$, the numerator of (17) becomes simpler, while we cannot ignore $\sqrt{\frac{U_E}{U_{AE}}}$ versus 1 in the denominator of (17). By this approximation, (17) is simplified to (18). Then we can write (17) as

$$\varphi(\lambda^*) \approx \frac{1 + \rho U_B}{(1 + \sqrt{\frac{U_E}{U_{AE}}})^2}. \tag{18}$$

Our objective is thus to maximize R_s in (12) by sequentially optimizing the diagonal phase shift matrix θ, and the TPC vector W of A. The problem is formulated as follows

$$\max_{\theta, W} R_s = \log_2(1 + \rho U_B) - 2\log_2(1 + \sqrt{\frac{U_E}{U_{AE}}}). \tag{19}$$
$$\text{s.t. } \theta = \text{diag}(e^{j\theta_1}, e^{j\theta_2}, ..., e^{j\theta_M})$$

Solving the problem (19) alternatively is also optimal. To justify this, we mention that Cui *et al.* [15] maximize the secrecy rate of the legitimate communication link by jointly designing the BS's transmit beamforming and the RIS's passive beamforming. Even though the resultant optimization problem is difficult to solve, they proposed an efficient algorithm for finding a suboptimal solution for it by applying the popular alternating optimization and semidefinite relaxation methods. Furthermore, aiming to enhance the secrecy rate, by jointly optimizing the transmit beamforming in conjunction with AN, and the RIS-aided passive beamforming, Guan *et al.* [16] proposed an efficient algorithm based on alternating optimization to solve the problem sub-optimally. Note that in the cost function of (19), we have dropped the operator

$[.]^+$ without loss of optimality since the optimal value of the problem has to be non-negative [15]. Based on the assumption that both A and the RIS are equipped with a large number of elements, LoS components are dominant between A and the RIS. Then the A-RIS channel is characterized by a rank-one geometric channel model that has been used for characterizing the mmWave channel [3], [6], [19], [43]

$$\boldsymbol{H}_{\mathrm{AI}} = \sqrt{NM\varrho_A\varrho_{I_1}\beta_{\mathrm{AI}}}r_{\mathrm{L}}\boldsymbol{a}_{\mathrm{M}}(\theta_{\mathrm{AOA},1})\boldsymbol{a}_{\mathrm{N}}^{\mathrm{H}}(\theta_{\mathrm{AOD},1}), \quad (20)$$

where $\theta_{\mathrm{AOA},1}$ is the azimuth angle of arrival (AoA) of the ULA at the RIS, and $\theta_{\mathrm{AOD},1}$ is the azimuth angle of departure (AoD) from the ULA at A. Moreover, $\boldsymbol{a}_{\mathrm{M}}(.) \in C^{\mathrm{M}}$ and $\boldsymbol{a}_{\mathrm{N}}(.) \in C^{\mathrm{N}}$ represent the normalized receive and transmit array response vectors at the RIS and A, respectively. In our work, ϱ_A and ϱ_{I_1} which represent the transmit and receive antenna element gains at A and at the RIS, respectively, are set to 9.82 dBi and 0 dBi, respectively. Furthermore, β_{AI} is the path loss between A and the RIS, which is set to $10^{-0.1(a+10b\log_{10}(d_{\mathrm{AI}}))}$, [6], [43], where $a = 61.4$, $b = 2$, as proposed by real-world channel measurements at 28 GHz [1]. Note that N and M are the numbers of antennas at A and the number of elements at the RIS, respectively. The complex gain r_{L} is generated according to a complex Gaussian distribution [1] as

$$r_{\mathrm{L}} \sim CN(0, \sigma_{\mathrm{L}}^2), \quad (21)$$

where we have $\sigma_{\mathrm{L}} = 5.8$ dB.

The RIS-B and RIS-E channels are modeled according to the following geometric channel model [1], [19], which has been extensively used for modeling mmWave channels

$$\boldsymbol{h}_{Ij} = \sqrt{\frac{M}{L_j}} \sum_{l=1}^{L_{Ij}} \sqrt{\varrho_{I_2}\varrho_j\beta_{Ij}}\alpha_{j,l}\boldsymbol{a}_{\mathrm{M}}(\theta_{\mathrm{AOD},2,\mathrm{I}}), j \in \{B, E\}, \quad (22)$$

where L_{IB} and L_{IE} are the numbers of paths associated with B and E, respectively. Furthermore, $\theta_{\mathrm{AOD},2,\mathrm{I}}$ is the AoD associated with the RIS-B link. Still referring to (22) $\boldsymbol{a}_{\mathrm{M}} \in C^{\mathrm{M}}$ represents the normalized transmit array response vector, ϱ_j and ϱ_{I_2} are the receive antenna element gain of node j, and the transmit antenna element gain of the RIS, which are set to 9.82 dBi and 0 dBi according to [6]. To elaborate further on (22), β_{Ij} is the path loss between RIS and node j which is set to $10^{-0.1(a+10b\log_{10}(d_{Ij}))}$, where $a = 72$, and $b = 2.92$, [1], while d_{Ij}, is the distance between the RIS and the receiver. The complex gain $\alpha_{j,l}$ is modeled by following the complex Gaussian distribution similar to (21) with $\sigma = 8.7$ dB.

In this part, we proceed to fined the optimal solution and then derive the ESR of the optimized network. In problem (19), the constraint only contains the variable $\boldsymbol{\theta}$. This motivates us to solve the Problem (19) by optimizing $\boldsymbol{W}$ and $\boldsymbol{\theta}$ alternatively. For a fixed $\boldsymbol{\theta}$, to maximize the ESR, it is clear that the optimal TPC vector $\boldsymbol{W}$, also known as maximum ratio transmission (MRT) is adopted [6], [43], and the optimal solution is given by

$$\boldsymbol{W}^* = \frac{(\boldsymbol{h}_{\mathrm{IB}}^{\mathrm{H}}\boldsymbol{\theta}\boldsymbol{H}_{\mathrm{AI}})^{\mathrm{H}}}{\|\boldsymbol{h}_{\mathrm{IB}}^{\mathrm{H}}\boldsymbol{\theta}\boldsymbol{H}_{\mathrm{AI}}\|}. \quad (23)$$

We mention that, the seminal papers [3], [6], and [43]–[45] have used the MRT as an optimal beamforming solution in their systems. To reflect on a philosophical note first, there are numerous optimal solutions, in fact, as many as the number of objective functions (OFs). Very often there is a trade-off, for example, between say the systems having the highest throughput and the highest power-efficiency, where both systems are optimal, but in terms of different OFs. We also remark that MRT is indeed AN optimal, but not the optimal solution. To clarify the issue further, we note that for any given phase shifts of RIS, it can be verified that the MRT is an optimal transmit beamforming solution [44]. Referring to [45], this conclusion can be readily extended to the case of hardware impairments. Moreover, the objective of [6] is to maximize the received signal power at MU, by jointly optimizing the transmit precoding (TPC) vector at the BS and the phase shift parameters used by RISs. For this purpose, they used an optimal TPC vector as an MRT solution.

Then, we solve Problem (19) for optimizing $\boldsymbol{\theta}$ as follows

Proposition 2: Assume $\boldsymbol{\theta}$, $\boldsymbol{H}_{\mathrm{AI}}$, and $\boldsymbol{h}_{\mathrm{IB}}$ are defined as in (1), (20), and (22), respectively. Then the optimal $\boldsymbol{\theta}^*$ that maximizes R_{s} and the related U_{B} are given by

$$\boldsymbol{\theta}^* = 2\pi\frac{d}{\lambda_{\mathrm{L}}}(m-1)(\sin\theta_{\mathrm{AOD},2,\mathrm{I}} - \sin\theta_{\mathrm{AOA},1}), \quad (24)$$

$$U_{\mathrm{B}} = a_{\mathrm{B}}\xi_{\mathrm{B}}, \quad (25)$$

where $\xi_{\mathrm{B}} = \left(\frac{\sum_{l=1}^{L_{\mathrm{IB}}}\alpha_{\mathrm{B},l}^*r_{\mathrm{L}}}{L_{\mathrm{IB}}}\right)^2$, $a_{\mathrm{B}} = NM^2\varrho_A\varrho_{I_1}\varrho_{I_2}\varrho_B\beta_{\mathrm{AI}}\beta_{\mathrm{IB}}$. Furthermore, λ_{L} is the mmWave wavelength, and d is the array element spacing.

Proof. Upon substituting (20), (22), and (23) into (8), we have $U_{\mathrm{B}} = NM^2\varrho_A\varrho_{I_1}\varrho_{I_2}\varrho_B\beta_{\mathrm{AI}}\beta_{\mathrm{IB}}\left(\frac{|\sum_{l=1}^{L_{\mathrm{B}}}\alpha_{\mathrm{B},l}^*r_{\mathrm{L}}|}{L_{\mathrm{IB}}}z\right)^2$, $z = \boldsymbol{a}_{\mathrm{M}}^{\mathrm{H}}(\theta_{\mathrm{AOD},2,\mathrm{I}})\boldsymbol{\theta}\boldsymbol{a}_{\mathrm{M}}(\theta_{\mathrm{AOA},1}))$. For maximizing U_{B}, it can be shown that the optimal phase shift angles that maximize z are obtained as seen in (24), which gives U_{B} of (25). ∎

Remark 2: Using [18, Lemma 1], the CDF of ξ_{B} is approximately represented by $F_{\xi_{\mathrm{B}}}(x) \simeq \frac{1}{\Gamma(L_{\mathrm{IB}}\mu)}\gamma(L_{\mathrm{IB}}\mu, \frac{\sqrt{x}}{\upsilon})$, where $\mu = \frac{\pi^2}{16-\pi^2}$ and $\upsilon = \frac{16-\pi^2}{4\pi}\sigma_{\mathrm{L}}\sigma$. Furthermore, $\gamma(.,.)$ and $\Gamma(.)$ represent the lower incomplete Gamma function and the Gamma function, respectively.

By using *Remark 2*, the CDF of U_{B} is given as

$$F_{U_{\mathrm{B}}}(x) \simeq \frac{1}{\Gamma(L_{\mathrm{IB}}\mu)}\gamma\left(L_{\mathrm{IB}}\mu, \frac{\sqrt{\frac{x}{a_{\mathrm{B}}}}}{\upsilon}\right). \quad (26)$$

Proposition 3: Assume, $\boldsymbol{H}_{\mathrm{AI}}$, $\boldsymbol{h}_{\mathrm{IE}}$, $\boldsymbol{W}^*$ and $\boldsymbol{\theta}^*$ are defined as seen in (20), (22), (23), and (24), respectively, while U_{E} of (11) is obtained as

$$U_{\mathrm{E}} = a_{\mathrm{E}} \xi_{\mathrm{E}}, \tag{27}$$

where $\xi_{\mathrm{E}} = \left(\frac{\sum_{l=1}^{L_{\mathrm{IE}}} \alpha_{\mathrm{E},l}^* r_{\mathrm{L}}}{L_{\mathrm{IE}}} \right)^2$, $a_{\mathrm{E}} = NM^2 \varrho_A \varrho_{I_1} \varrho_{I_2} \varrho_E \beta_{\mathrm{AI}} \beta_{\mathrm{IE}}$, and L_{IE} is the number of paths received by E.

Proof. For a large M and by using [18] and [46], we can approximate ξ_{E} as a random variable with gamma distribution, where the CDF of ξ_{E} can be derived as $F_{\xi_{\mathrm{E}(x)}} = \frac{1}{\Gamma(L_{\mathrm{IE}})} \gamma \left(L_{\mathrm{IE}}, \frac{x}{\sigma_{\mathrm{E}}^2} \right)$ with $\sigma_{\mathrm{E}} = 10^{0.58} \times 10^{0.87}$. ∎

Assuming that A transmits AN with the aid of MRT beamforming for contaminating the reception of E, U_{AE} in (10) is written as follows

$$U_{\mathrm{AE}} = \|\boldsymbol{h}_{\mathrm{AE}}\|^2. \tag{28}$$

For mathematical simplicity, we assume that the CSI of the E in A is known.

Now, by using the channel model of (22), the random variable U_{AE} can be obtained approximately as

$$U_{\mathrm{AE}} = a_{\mathrm{AE}} \left(\frac{\sum_{l=1}^{L_{\mathrm{AE}}} \alpha_{\mathrm{E},l}}{L_{\mathrm{AE}}} \right)^2 = a_{\mathrm{AE}} \xi_{\mathrm{AE}}, \tag{29}$$

where we have $a_{\mathrm{AE}} = NM^2 \varrho_A \varrho_{I_1} \varrho_{I_2} \varrho_E \beta_{\mathrm{AI}} \beta_{\mathrm{IE}}$ and L_{AE} is the total AN paths towards E.

Now we examine the CDF of the perfect hardware based scheme of $\sqrt{\frac{U_{\mathrm{E}}}{U_{\mathrm{AE}}}}$, denoted by $F^{\mathrm{P}}_{\sqrt{\frac{U_{\mathrm{E}}}{U_{\mathrm{AE}}}}}(x)$ as follows. Upon using (27), and (29), we have $\sqrt{\frac{U_{\mathrm{E}}}{U_{\mathrm{AE}}}} = \sqrt{\frac{\xi_{\mathrm{E}}}{\xi_{\mathrm{AE}}}}$. For $F^{\mathrm{P}}_{\sqrt{\frac{U_{\mathrm{E}}}{U_{\mathrm{AE}}}}}(x)$, we have

$$F^{\mathrm{P}}_{\sqrt{\frac{U_{\mathrm{E}}}{U_{\mathrm{AE}}}}}(x) = \int_0^\infty F^{\mathrm{P}}_{\sqrt{\xi_{\mathrm{E}}}}(x^2 y) f^{\mathrm{P}}_{\sqrt{\xi_{\mathrm{AE}}}}(y) dy. \tag{30}$$

By relying on *Proposition 3* for the CDF of ξ_{E}, we arrive $F_{\xi_{\mathrm{AE}}}(x) \simeq \frac{1}{\Gamma(L_{\mathrm{AE}})} \gamma \left(L_{\mathrm{AE}}, \frac{x}{\sigma_{\mathrm{E}}^2} \right)$, Furthermore, we can extract the pdf of ξ_{AE} as $\xi_{AE} \sim \Gamma(L_{\mathrm{AE}}, \sigma_{\mathrm{E}}^2)$. Now, after substituting these into (30), and using [47, 6.455.2], a closed-form expression is obtained for the CDF of the perfect hardware scheme as

$$F^{\mathrm{P}}_{\sqrt{\frac{\xi_{\mathrm{E}}}{\xi_{\mathrm{AE}}}}}(x) = \frac{x^{2L_{\mathrm{IE}}}}{B(L_{\mathrm{IE}}, L_{\mathrm{AE}}) L_{\mathrm{IE}} (x^2 + 1)^{L_{\mathrm{IE}} + L_{\mathrm{AE}}}}$$
$$\times {}_2F_1(1, L_{\mathrm{IE}} + L_{\mathrm{AE}}; L_{\mathrm{IE}} + 1; \frac{x^2}{x^2 + 1}), \tag{31}$$

where $B(x, y)$ is the beta function [47, 8.384.1] and ${}_2F_1(a, b; c; z)$ is the Gauss hypergeometric function [47, 9.100].

Following (19), and by using (26) and (31), the ESR of the perfect hardware associated with AN-aided transmission via

the RIS can be written as

$$\bar{R}_s^{\mathrm{P}} = \frac{1}{\ln 2} \tag{32}$$
$$\times \left\{ \int_0^\infty \frac{\frac{\Gamma\left(L_{\mathrm{IB}}\mu, \frac{\sqrt{\frac{x}{\rho a_{\mathrm{B}}}}}{\upsilon} \right)}{\Gamma(L_{\mathrm{IB}}\mu)}}{1 + x} dx - 2 \int_0^\infty \frac{1 - F^{\mathrm{P}}_{\sqrt{\frac{U_{\mathrm{E}}}{U_{\mathrm{AE}}}}}(x)}{1 + x} dx \right\}.$$

The derived ESR expression in (32) states that the ESR increases when ρ and N increase. Because the gap between the ESRs of the legitimate and eavesdropping nodes increases, when ρ and N increase. However, when ρ and N are large enough, the ESR is mainly determined by these parameters, and the ESR gap between the legitimate and eavesdropping nodes tends to be constant. By increasing the number of paths between the RIS and the user i.e., L_{IB}, the value of the upper incomplete gamma function in the first sentence of (32) is increased, leading to ESR increment, where the number of L_{IB} is increased by reducing the blockage effects of the environment. As such, increasing the number of antennas and the resultant antenna gain in the transmitter node increases the scale parameter in the upper incomplete gamma function in the first sentence of (32), hence, leading to an increase in the first term of (32) and thereby, to an ESR improvement. Furthermore, an increase in the multiplication factor of $\beta_{\mathrm{AI}} \beta_{\mathrm{IB}}$, which has resulted from the reduced distances in the first or second hop of the legitimate nodes, leads to an increase in the parameter a_{B} of (32) and consequently, to an increase in the ESR.

B. Imperfect Hardware Analysis

In the presence of HWIs, we observe that due to the transmission of AN towards the Eve and as a benefit of our active and passive beamformers transmitting the designed signal from A to B, the information leakage U_{E} is relatively small compared to U_{AE}, i.e., $\frac{U_{\mathrm{E}}}{U_{\mathrm{AE}}} < 1$. Hence, due to the small values of k_{A} and k_{B}, we omitted the values of $\sqrt{\frac{U_{\mathrm{E}}}{U_{\mathrm{AE}}}}(1 + \rho U_{\mathrm{B}}(k_{\mathrm{A}}^2 + k_{\mathrm{B}}^2))$ compared to ρU_{B} in the numerator of φ in (14). Given the symbol values conveying the data, it is clear that the denominator of (14) can also be approximated as $\sqrt{\rho(k_{\mathrm{A}}^2 + k_{\mathrm{B}}^2) \frac{U_{\mathrm{E}}}{U_{\mathrm{AE}}} U_{\mathrm{B}}}$. As a result, in this case, φ of (14) can be approximated as

$$\varphi(\lambda^*) \approx \frac{1 + \rho U_{\mathrm{B}}}{\left(1 + \sqrt{\rho(k_{\mathrm{A}}^2 + k_{\mathrm{B}}^2) \frac{U_{\mathrm{E}}}{U_{\mathrm{AE}}} U_{\mathrm{B}}} \right)^2}. \tag{33}$$

For calculating the ESR, we define $\sqrt{\rho(k_{\mathrm{A}}^2 + k_{\mathrm{B}}^2) \frac{U_{\mathrm{E}}}{U_{\mathrm{AE}}} U_{\mathrm{B}}} = c\sqrt{\frac{\xi_{\mathrm{E}}}{\xi_{\mathrm{AE}}} \xi_{\mathrm{B}}}$ where $c = \sqrt{\rho(k_{\mathrm{A}}^2 + k_{\mathrm{B}}^2) \frac{a_{\mathrm{E}}}{a_{\mathrm{AE}}} a_{\mathrm{B}}}$, and then we examine the CDF of $c\sqrt{\frac{\xi_{\mathrm{E}}}{\xi_{\mathrm{AE}}} \xi_{\mathrm{B}}}$. By exploiting the law of total probability and since the variables ξ_{B}, ξ_{E} and ξ_{AE} are independent, and using [48, 2.10.1.12] and [47, 3.326.2], we

obtain a closed-form expression for the CDF of $c\sqrt{\frac{\xi_E}{\xi_{AE}}}\xi_B$ as

$$F^{IP}_{c\sqrt{\frac{\xi_E}{\xi_{AE}}}\xi_B}(x) \tag{34}$$

$$= \frac{1}{\Gamma(L_{IB}\mu)\Gamma(L_{IE})\Gamma(L_{AE})}\left\{(\frac{x}{c\upsilon})^{L_{IB}\mu}\Omega_1 + (\frac{x}{c\upsilon})^{2L_{IE}-2}\Omega_2\right\},$$

where

$$\Omega_1 = \sum_{k=1}^{\infty}[(-1)^{k+1}\frac{\Gamma\big(-\frac{L_{IB}\mu+k-2(L_{IE}-1)}{2}\big)}{k!(L_{IB}\mu+k)}(\frac{x}{c\upsilon})^k\Gamma(\varsigma_B)],$$

$$\Omega_2 = \sum_{k=1}^{\infty}[(-1)^{k+1}\frac{\Gamma\big(L_{IB}\mu-2(L_{IE}+k-1)\big)}{k!(L_{IE}+k-1)}(\frac{x}{c\upsilon^2})^k\Gamma(\varsigma_E)],$$

where we have $\varsigma_B = \frac{L_{IB}\mu+2(L_{AE}+1)+k}{2}$ and $\varsigma_E = L_{IE}+L_{AE}+k$.

Now taking HWIs into account, the ESR can be derived similar to (32) as

$$\bar{R}^{IP}_s = \frac{1}{\ln 2} \tag{35}$$

$$\times\left\{\int_0^{\infty}\frac{\frac{\Gamma\big(L_{IB}\mu,\frac{\sqrt{\frac{x}{\rho a_B}}}{\upsilon}\big)}{\Gamma(L_{IB}\mu)}}{1+x}dx - 2\int_0^{\infty}\frac{1-F^{IP}_{c\sqrt{\frac{\xi_E}{\xi_{AE}}}\xi_B}(x)}{1+x}dx\right\}.$$

The conclusions mentioned about (32) are valid for (35). Furthermore, by increasing the HWIs, the value of $F^{IP}_{c\sqrt{\frac{\xi_E}{\xi_{AE}}}\xi_B}(x)$ in the second term of (35) is reduced resulting the ESR reduction. Moreover, by comparing (32) and (35), it is deduced that for the system having perfect hardware, according to (32), only the first term of (32) increases by increasing the transmit power of the signal. However, for the system having HWIs, both terms of (35) are increased. In this case, the ESR experiences a smaller increase than the perfect hardware. Therefore, the presence of HWIs even in AN-aided systems causes a reduction in the secrecy performance of wireless systems.

IV. HARDWARE DESIGN

In this section, we turn our attention to the RF imperfections of an RIS-assisted network for maximizing the ESR. Towards our goal, we optimally distribute the total tolerable hardware impairments, $k_A + k_B = k_{total}$, between A and B in the network. From an engineering perspective, depending on the specified cost of each active network node, we show how the transmission and reception RF chains should be designed for maximizing the ESR. Therefore, we should find k_A and k_B maximizing the ESR, so that $k_A + k_B = k_{total}$.

By substituting $k_A = k_{total} - k_B$ into $\varphi(\lambda^*)$ of (33), and taking the first-order derivative of (33) with respect to k_B, the optimal level of HWI in the legitimate receiver can be obtained by solving the following equation

$$\frac{\partial\varphi}{\partial k_B} = \frac{\rho U_E U_B}{U_{AE}}\big(-2k_{total}+4k_B\big) \tag{36}$$

$$\times\Big(2+\sqrt{\frac{U_E}{U_{AE}}\big(1+\rho U_B((k_{total}-k_B)^2+k_B^2)\big)}\Big) = 0,$$
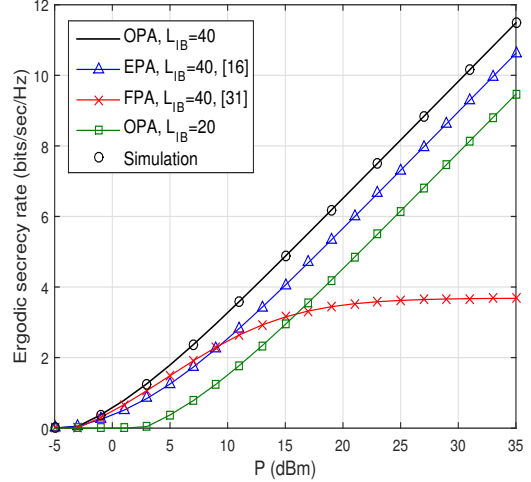
Fig. 3: The impact of P on the ESR performance with perfect hardware assuming $L_{IE} = 10$, $N = 32$, $M = 50$.

where $\varphi(\lambda^*)$ is a concave function of k_B in the feasible set. After calculating the roots of (36), a single solution can be obtained as

$$k_A^* = k_B^* = \frac{k_{total}}{2}. \tag{37}$$

Again, we conclude from (37) that by optimally distributing the HWIs between the transmission and reception RF chains at A and B, the secrecy performance is increased.

V. SIMULATIONS RESULTS

We now present our simulation results characterizing the performance of the alternating OPA and beamforming design of the proposed RIS-assisted secure transmission scheme. The BS employs a ULA having N antennas, and the RIS consists of a ULA with M reflecting elements. The array element spacing for both the ULA and RIS is assumed to be $d = \frac{\lambda_L}{2}$ [12]. Unless otherwise stated, we set $N = 32$, $M = 50$, and $\sigma_n^2 = -105$ dBm. The simulation parameters are given as follows. P is the total transmit power at A. Information signal sent by A has the power of λP, and the AN the power of $(1-\lambda)P$, where λ is the power sharing factor. The OPA factor is obtained from (13). Furthermore, ϱ_A, ϱ_{I_1}, ϱ_{I_2}, ϱ_B and ϱ_E are respectively set to be 9.82 dBi, 0 dBi, 9.82 dBi, 0 dBi and 0 dBi for both the BS-RIS channel and for the RIS-node j channel, where $j \in \{B, E\}$. Moreover, the path-loss between A and the RIS is set to $10^{-0.1(a+10b\log_{10}(d_{AI}))}$, where d_{AI} is the distance between A and the RIS. Note that the values of a, b are $a = 61.4$ and $b = 2$. Furthermore, the path-loss between the RIS and node j, $j \in \{B, E\}$ is set to $10^{-0.1(a+10b\log_{10}(d_{Ij}))}$, where d_{Ij} is the distance between the RIS and node j. Note that the values of a, b are $a = 72$ and $b = 2.92$. Moreover, r_L and $\alpha_{j,l}$ are generated according to complex Gaussian distributions as $r_L \sim CN(0, \sigma_L^2)$, and $\alpha_{j,l} \sim CN(0, \sigma^2)$, where we have $\sigma_L = 5.8$ dB and $\sigma = 8.7$ dB. The AOAs/AODs of the clusters are assumed to obey the uniform distribution.
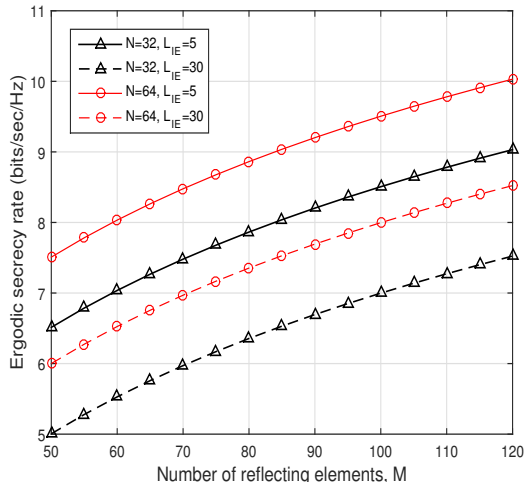
Fig. 4: ESR versus the number of reflecting elements, M, for our proposed scheme with $P = 20$ dBm, and perfect hardware.

Fig. 5: ESR versus P, for the our proposed schemes and different values of k_A and k_B, under perfect and imperfect hardware schemes assuming $N = 32$, $M = 50$.

Fig. 2 shows the impact of P on the ESR performance of the proposed RIS-aided secure scheme. Our observations are summarized as follows:

- By assigning AN for A, the ESR increases with respect with P. This is because AN degrades the eavesdropping link and hence increases the achievable secrecy rate.
- When the OPA is applied at A, the highest ESR is obtained comparing with the equal power allocation (EPA), i.e., $\lambda = \frac{1}{2}$ [16], and full power allocation (FPA), i.e., $\lambda = 1$ [35], techniques. For example, for the EPA at A, the ESR decreases by about 1 bit/sec/Hz with respect to the OPA strategy.
- The highest ESR is related to the highest number of paths of the RIS-B link. i.e., increased blockage causes a reduction in the number of paths which in turn leads to a reduction in the ESR.
- At high powers, canceling the AN leads to a sharp reduction in ESR, while at low powers, this cancelation has little effect on the ESR. The reason behind this behavior is that at a low P, the eavesdropping capability of E is significantly reduced. In other words, the AN-based scheme increases the ESR performance compared to the FPA strategy. For instance, with $M = 32$ and $N = 50$, this gain is about 5 bits/sec/Hz at $P = 15$ dBm and about 10 bits/sec/Hz at $P = 30$ dBm.

Fig. 3 plots the ESR versus the number of passive reflecting elements M at the RIS. Our observations are summarized as follows:

- It is observed that the ESR achieved by our proposed scheme increases more steeply with M for smaller values and then rises slightly for larger M. This is because when M increases, it can also improve the reception at the E, which leads to a slower ESR improvement.
- Furthermore, increasing N from 32 to 64 increases the ESR.
- It is also observed that When E is placed far from the paths transmitted to B by the RIS, it is obvious that the
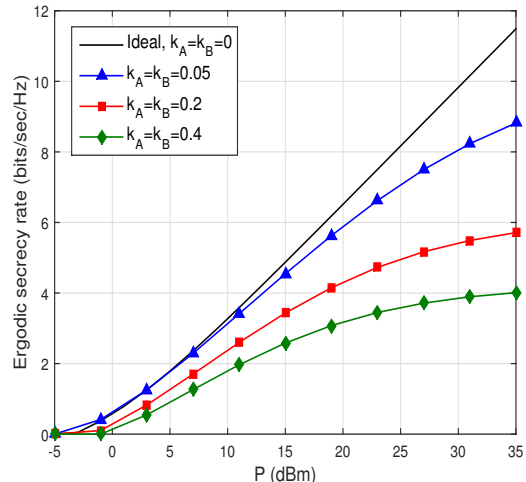
ESR improves with the increase of N. It is expected that when E is placed close to the paths transmitted to B by the RIS, the performance gain of the ESR decreases with the increase of N, compared to the previous state. But we can see from the Fig. 3 that this performance gain doesn't decrease. The reason is that according to (19), the amount of eavesdropping is proportional to $\frac{U_E}{U_{AE}}$, which is independent of P, ϱ_E, ϱ_A, and N, which makes our AN-aided scheme effective in improving the ESR in such challenging compromised scenarios.

In Fig. 4, the ESR is depicted as a function of P for our proposed scheme. Different values of k_A and k_B, are considered, and we assume $L_{IB} = 40$, $L_{IE} = 5$. Again, the circles represent the Monte Carlo simulation results, while the curves associated with the analytical results are evaluated from (32) and (35). As a benchmark, the ESR versus P for the perfect hardware case is also plotted. As expected, when P increases, the ESR also increases. However, in the case of imperfect hardware cases, the ESR saturates. As a result, since the ESR is determined by the level of imperfections, it increases as k_A and k_B decreases. Moreover, we observe that the hardware imperfections have a negligible effect on the ESR in the low-P regime, whereas, in the high-P regime, their impact is more harmful.

Fig. 5 reveals the secrecy performance advantage of the proposed OPA scheme compared to the EPA and FPA techniques, associated with $\lambda = 0.5$ and $\lambda = 1$, respectively, in the case of imperfect hardware. It is also observed that the ESR decreases when E is placed close to the paths transmitted to B by the RIS, and the amount of this reduction increases with P.

Moreover, according to Figs. 4 and 5, we can see that HWIs reduce the ESR, especially at higher powers, and we conclude that AN cancellation also causes a sharp decrease in the ESR. By comparing the figures, we understand that AN cancellation has a more significant effect on reducing ESR compared to increasing the level of HWIs. In other words,
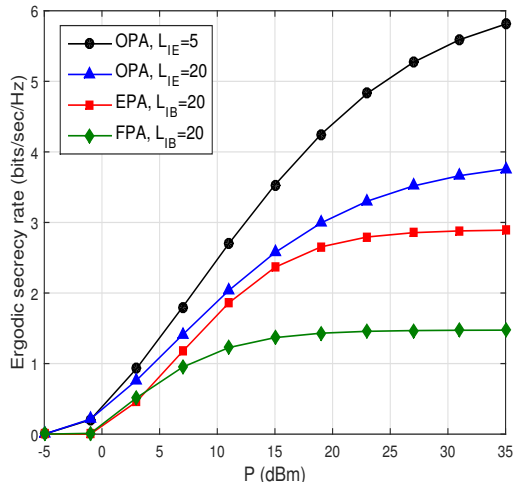
Fig. 6: ESR versus P for different techniques under HWI with $k_A = k_B = k_E = 0.4$, assuming $N = 32$, $M = 50$.
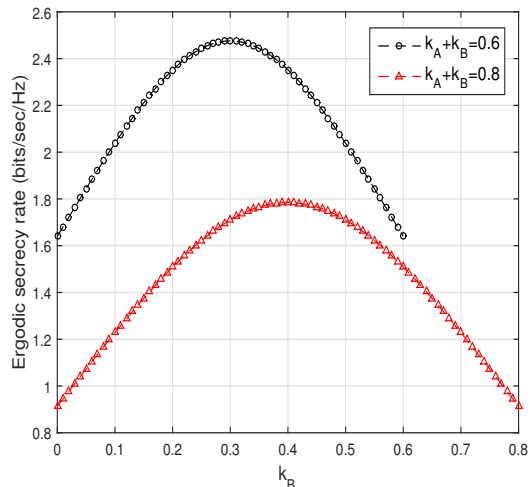
Fig. 7: ESR versus k_B for the two different hardware imperfection designs, with $P = 20$ dBm, assuming $N = 32$, $M = 50$.

if we use hardware with a higher imperfection and do not use AN, the ESR will decrease drastically. To compensate for this decrease, AN injection assists to increase the ESR to an acceptable value.

Fig. 6 shows the ESR as a function of EVM at B for $P = 20$ dBm, $N = 32$, $M = 50$ for two cases of $k_{total} = 0.6$ and 0.8. As we can see in Fig. 6, the optimal distribution of hardware impairments between A and B is 50%. In other words, these results confirm our mathematical analytics, suggesting that it is better to employ a transmitter and a receiver that are both of medium hardware impairment. This reduces the cost of hardware. We note that in order to shed light on the system design, as you can see from Fig 6, for the scenario with ideal hardware for the user node ($k_A = k_{total}, k_B = 0$) and the case, when the transmitter has ideal hardware ($k_A = 0, k_B = k_{total}$), the secrecy performance is not good at its best. But the improved ESR performance is obtained by appropriately designing the HWIs, i.e., by potentially investing more funds into buying

hardware components.

VI. CONCLUSIONS

The effects of transceiver hardware impairments on the secrecy performance of an RIS-assisted mmWave system were investigated, where a multi-antenna A transmits confidential messages to a single-antenna B in the presence of a single antenna passive eavesdropper. We first introduced a general model that takes into account the transceiver hardware impairments. In order to increase the ESR by employing AN in the system, we presented a scheme for optimizing the signal and AN powers, using an appropriate TPC at A and designing the optimal phase shifts at the RIS for improving the ESR. Additionally, we calculated closed-form expressions for the CDFs of the received SNRs at the legitimate and eavesdropping nodes in order to calculate the ESR performance. Furthermore, we conclude that AN cancellation has a more significant effect on reducing ESR compared to increasing the level of HWIs. In other words, if we use hardware with a higher imperfection and do not use AN, the ESR will decrease drastically. To compensate for this decrease, AN increases the ESR to an acceptable value. Moreover, we improved the ESR of the system by optimizing the corresponding hardware design. The results illustrate that by beneficially distributing the tolerable HWIs between the transmission and reception RF chains, the system's secrecy rate can be improved. Moreover, increased blockage causes a reduction in the number of paths which in turn leads to a reduction in the ESR. Our numerical examples also show that the proposed design provides a robust improvement against blockage in mmWave communications. As for future work, it would be interesting to extend the results in this paper to the case, where a relay node also exists in the network. For ease of exposition and make a sensible conclusion, the quantitative results are summarized in Table IV.

REFERENCES

[1] M. Riza Akdeniz, Y. Liu, M. K. Samimi, S. Sun, S. Rangan, T. S. Rappaport, and E. Erkip, "Millimeter wave channel modeling and cellular capacity evaluation," *IEEE J. Sel. Areas Commun.*, vol. 32, no. 6, pp. 164–1179, Jun. 2014.

[2] Q. Wu and R. Zhang, "Intelligent reflecting surface enhanced wireless network via joint active and passive beamforming," *IEEE Trans. Wireless Commun.*, vol. 18, no. 11, pp. 5394–5409, Nov. 2019.

[3] Y. Han, W. Tang, S. Jin, C.-K. Wen, and X. Ma, "Large intelligent surface-assisted wireless communication exploiting statistical CSI," *IEEE Trans. Veh. Technol.*, vol. 68, no. 8, pp. 8238–8242, Aug. 2019.

[4] S. Gong, C. Xing, S. Wang, L. Zhao, and J. An, "Throughput maximization for intelligent reflecting surface aided MIMO WPCNs with different DL/UL reflection patterns," *IEEE Trans. Signal Process.*, vol. 69, pp. 2706–2724, 2021.

[5] X. Zhai, G. Han, Y. Cai, and H. Hanzo, "Beamforming design based on Two-stage stochastic optimization for RIS-assisted over-the-air computation systems," *IEEE Internet of Things Journal*, vol. 9, no. 9, pp. 5474–54 881, 2022.

[6] P. Wang, J. Fang, X. Yuan, Z. Chen, H. Duan, and H. Li, "Intelligent reflecting surface-assisted millimeter wave communications: Joint active and passive precoding design," *IEEE Trans. Veh. Technol.*, vol. 69, no. 12, pp. 14 960–14 973, Dec. 2020.

[7] M. Forouzesh, P. Azmi, A. Kuhestan, and P. L. Yeoh, "Joint information-theoretic secrecy and covert communication in the presence of an untrusted user and warden," *IEEE Internet of Things Journal*, vol. 8, no. 9, pp. 7170–7181, May. 2021.

TABLE IV: Brief Review of Quantitative Results.

- The authors of [13], [27] and [41], have only considered the effect of transceiver HWIs. In like with these, we focussed our attention on the effect of transceiver HWIs in our paper.
- For a system model in the absence of HWIs, we present optimal solutions for the signal and AN powers, the beamforming design at the BS, and the phase shifts of the RIS elements.
- For this case, closed-form expressions are derived for the cumulative distribution functions of the signal-to-noise-ratios experienced both at the legitimate and eavesdropping nodes. Then, a compact solution is presented for the ergodic secrecy rate (ESR) performance.
- At the next step, we extend our design and analysis by considering the HWIs of the radio-frequency (RF) modules of the BS, MU and Eve.
- Our results highlight the detrimental impact of HWIs on the achievable ESR.
- We demonstrated that the ESR can be further increased by beneficially distributing the tolerable HWIs between the transmission and reception RF chains.
- The results illustrate that by beneficially distributing the tolerable HWIs between the transmission and reception RF chains, the system's secrecy rate can be improved.
- The proposed design provides a robust improvement against blockage in mmWave communications.

[8] M. T. Mamaghani, A. Kuhestani, and H. Behroozi, "Can a multi-hop link relying on untrusted amplify-and-forward relays render security?" *Wireless Networks*, vol. 27, pp. 795–807, Jan. 2021.

[9] M. Ragheb, A. Kuhestani, S. M. Safavi Hemami, D. W. K. Ng, and L. Hanzo, "On the physical layer security of untrusted millimeter wave relaying networks: A stochastic geometry approach," *IEEE Trans. Inf. Forens. and Security*, vol. 17, pp. 53–68, Oct. 2021.

[10] M. Ragheb and S. M. Safavi Hemami, "Secure transmission in large-scale cooperative millimeter-wave systems with passive eavesdroppers," *IET Commun*, vol. 14, no. 1, pp. 37–46, Jan. 2020.

[11] A. Kuhestani, A. Mohammadi, K.-K. Wong, P. L. Yeoh, and M. Moradikia, "Optimal power allocation by imperfect hardware analysis in untrusted relaying networks," *IEEE Trans. Wireless Commun.*, vol. 17, no. 7, pp. 4302–4314, Jul. 2018.

[12] S. Mashdour, M. Moradikia, and P. L. Yeoh, "Secure mm-Wave communications with imperfect hardware and uncertain eavesdropper location," *Trans. Emerg. Telecommun. Technol.*, vol. 31, no. 10, pp. 1–21, Oct. 2020.

[13] A. A. Boulogeorgos and A. Alexiou, "How much do hardware imperfections affect the performance of reconfigurable intelligent surface-assisted systems?" *IEEE Open J. of the Commun. Society*, vol. 1, pp. 1185–1195, Aug. 2020.

[14] Z. T. Tang, T. Hou, Y. L. Liu, J. Z. Zhang, and L. Hanzo, "Physical Layer Security of Intelligent Reflective Surface Aided NOMA Networks," *IEEE Trans. Veh. Technol.*, vol. 1.

[15] M. Cui, G. Zhang, and R. Zhang, "Secure wireless communication via intelligent reflecting surface," *IEEE Wireless Commun. Lett.*, vol. 8, no. 5, pp. 1410–1414, Oct. 2019.

[16] X. Guan, Q. Wu, and R. Zhang, "Intelligent reflecting surface assisted secrecy communication: Is artificial noise helpful or not?" *IEEE Wireless Commun. Lett.*, vol. 9, no. 6, pp. 778–782, Jun. 2020.

[17] H. Shen, W. Xu, S. Gong, Z. He, and C. Zhao, "Secrecy rate maximization for Intelligent reflecting surface assisted multi-antenna communications," *IEEE Wireless Commun. Lett.*, vol. 23, no. 9, pp. 1488–1492, Sep. 2019.

[18] L. Lv, Q. Wu, Z. Li, N. Al-Dhahir, and J. Chen, "Secure two-way communications via intelligent reflecting surfaces," *IEEE Wireless Commun. Lett.*, vol. 25, no. 3, pp. 744–748, Mar. 2021.

[19] J. Qiao and M. S. Alouini, "Secure transmission for intelligent reflecting surface-assisted mmWave and terahertz systems," *IEEE Wireless Commun. Lett.*, vol. 9, no. 10, pp. 1743–1747, Oct. 2020.

[20] L. Dong, H.-M. Wang, J. Bai, and H. Xiao, "Double intelligent reflecting surface for secure transmission with inter-surface signal reflection," *IEEE Trans. Veh. Technol.*, vol. 70, no. 3, pp. 2912–2916, Mar. 2021.

[21] X. Wu, J. Ma, C. Gu, X. Xue, and X. Zeng, "Robust Secure Transmission Design for IRS-Assisted mmWave Cognitive Radio Networks," *IEEE Trans. Veh. Technol.*, vol. 71, no. 8, pp. 8441–8456, Aug. 2022.

[22] E. N. Egashira, D. P. M. Osorio, N. T. Nguyen, and M. Juntti, "Secrecy Capacity Maximization for a Hybrid Relay-RIS Scheme in mmWave MIMO Networks," in *in Proc. IEEE 95th Vehicular Technology Conf. (VTC2022-Spring)*, 2022, pp. 1–6.

[23] M. Letafati, A. Kuhestani, and H. Behroozi, "Three-hop untrusted relay networks with hardware imperfections and channel estimation errors for Internet of Things," *IEEE Trans. Inf. Forens. and Security*, vol. 15, pp. 2856–2868, Mar. 2020.

[24] V. Shahiri, A. Kuhestani, and L. Hanzo, "Short-packet amplify-and-forward relaying for the internet-of-things in the face of imperfect channel estimation and hardware impairments," *IEEE Trans. Green. Commun. and Net.*, 2022.

[25] Y. Li, D. Tian, and J. Yang, "Study on IRS-assisted WPT communication system with phase errors," in *in Proc. Int. Conf. Computer and Commun. (ICCCS)*, 2022, pp. 571–576.

[26] I. Trigui, W. Ajib, and W. P. Zhu, "Secrecy outage probability and average rate of RIS-aided communications using quantized phases," *IEEE Commun. Lett.*, vol. 25, no. 6, pp. 1820–1824, Jun. 2021.

[27] M. H. N. Shaikh, V. A. Bohara, A. Srivastava, and G. Ghatak, "Performance analysis of intelligent reflecting surface-assisted wireless system with non-ideal transceiver," *IEEE Open J. of the Commun. Society*, vol. 2, pp. 671–686, 2021.

[28] A. Papazafeiropoulos, C. Pan, P. Kourtessis, and J. M. Senior, "Intelligent reflecting surface-assisted MU-MISO systems with imperfect hardware: Channel estimation and beamforming Design," *IEEE Trans. Wireless Commun.*, vol. 21, no. 3, pp. 2077–2092, Mar. 2022.

[29] J. Dai, F. Zhu, C. Pan, H. Ren, and K. Wang, "Statistical CSI-based transmission design for reconfigurable intelligent surface-aided massive MIMO systems with hardware impairments," *IEEE wireless commun. Lett.*, vol. 11, no. 1, pp. 38–42, Jan. 2022.

[30] N. D. Nguyen, A.-T. Le, M. Munochiveyi, F. Afghah, and E. Pallis, "Intelligent reflecting surface aided wireless systems with imperfect hardware," *Electronics*, vol. 11.

[31] Y. Liu, E. Liu, and R. Wang, "Energy efficiency analysis of intelligent reflecting surface system with hardware impairments," in *in Proc. IEEE Global Communications Conference (GLOBECOM)*, 2020, pp. 1–6.

[32] A. E. Canbilen, E. Basar, and S. S. Ikki, "On the performance of ris-assisted space shift keying: Ideal and non-ideal transceivers," *IEEE Trans. Commun.*, vol. 70, no. 9, pp. 5799–5810, Sept. 2022.

[33] C. Chen, M. Wang, B. Xia, Y. Guo, and J. Wang, "Performance Analysis and Optimization of IRS-Aided Covert Communication With Hardware Impairments," *IEEE Trans. Veh. Technol.*, vol. 72, no. 4, pp. 5463–5467, Apr. 2023.

[34] M. Tota Khel and K. A. Hamdi, "Secrecy Capacity of IRS-Assisted Terahertz Wireless Communications With Pointing Errors," *IEEE Wireless Commun. Lett.*, vol. 27, no. 4, pp. 1090–1094, Apr. 2023.

[35] X. Yu, D. Xu, and R. Schober, "Enabling secure wireless communications via intelligent reflecting surfaces," in *in Proc. IEEE Global Communications Conference (GLOBECOM)*. Washington, DC: IEEE, Dec. 2019, pp. 1–6.

[36] Y. Xiu, J. Zhao, C. Yuen, Z. Zhang, and G. Gui, "Secure beamforming for multiple intelligent reflecting surfaces aided mmWave systems," *IEEE Wireless Commun. Lett.*, vol. 25, no. 2, pp. 417–421, Feb. 2021.

[37] T. Rappaport and et al., "Wireless communications and applications above 100 GHz: Opportunities and challenges for 6G and beyond," *IEEE Access*, vol. 7, pp. 78 729–78 757, 2019.

[38] S. Atapattu, R. Fan, P. Dharmawansa, G. Wang, J. Evans, and T. A. Tsiftsis, "Reconfigurable intelligent surface assisted two–way communications: Performance analysis and optimization," *IEEE Trans. Commun.*, vol. 68, no. 10, pp. 6552–6567, Oct. 2020.

[39] Y. Cao and T. Lv, "Intelligent reflecting surface aided multi-user mmWave communications for coverage enhancement," in *Proc. 31th Annual International Symposium on Personal, Indoor and Mobile Radio Commun. (PIMRC)*, 2020, pp. 1–6.

[40] L. Dong and H. M. Wang, "Enhancing secure MIMO transmission via intelligent reflecting surface," *IEEE Trans. Wireless Commun.*, vol. 19, no. 11, pp. 7543–7556, Nov. 2020.

[41] Q. Chen, M-L Li, X. Yang, and R. Alturki, "Impact of Residual Hardware Impairment on the IoT Secrecy Performance of RIS-Assisted NOMA Networks," *IEEE Access*, vol. 9, pp. 42 583–42 592, Mar. 2021.

[42] Z. Peng, R. Weng, C. Pan, G. Zhou, M. Di Renzo, and A. Lee Swindlehurst, "Robust Transmission Design for RIS-assisted Secure Multiuser Communication Systems in the Presence of Hardware Impairments," *IEEE Trans. Wireless Commun.*

[43] F. Yang, J. Wang, H. Zhang, C. Chang, and J. Cheng, "Intelligent reflecting surface-assisted mmWave communication exploiting statistical CSI," in *in Proc. IEEE Int. Conf. Commun. (ICC)*, 2020, pp. 1–6.

[44] Q. Wu and R. Zhang, "Beamforming optimization for wireless network aided by intelligent reflecting surface with discrete phase shifts," *IEEE Trans. Commun.*, vol. 68, no. 3, pp. 1838–1851, Mar. 2020.

[45] E. Bjornson, J. Hoydis, M. Kountouris, and M. Debbah, "Massive mimo systems with non-ideal hardware: Energy efficiency, estimation, and capacity limits," *IEEE Trans. Inf. Theory*, vol. 60, no. 11, pp. 7112–7139, Nov. 2014.

[46] Y. Ju, H. Wang, T. Zheng, and Q. Yin, "Secure transmissions in millimeter wave systems," *IEEE Trans. Commun.*, vol. 65, no. 5, pp. 2114–2127, May. 2017.

[47] A. Jeffrey and D. Zwillinger, *Table of integrals, series, and products*. New York, NY: Elsevier, 2007.

[48] A. P. Prudnikov, Y. A. Brychkov, and O. Marichev, *Integrals and series*, USSR Academy of Sciences Moscow, 1986.